An Analysis of the UV, ORD, and CD Bandshapes of the DNA-Acridine Orange Complex by the Linear Response Polarizability Theory

Hirotoshi Ito and Yasumasa J. I'Haya*

Department of Materials Science, The University of Electro-Communications, Chofu-shi, Tokyo 182

(Received March 12, 1979)

The linear response polarizability theory of the spectral bandshapes is applied to the numerical analysis of the UV, ORD, and CD spectra of the DNA–Acridine Orange complex by using various models of conformation. In all calculations, we make use of an infinite orders approximation for the intermonomer electronic interaction, since convergence of the Dyson-type series for the polymer polarizability tensor sometimes becomes seriously slow, in particular in such case that the transition moments of a constituent monomer such as Acridine Orange are quite large. It is found that among the various outside-stacking models, a dimer-pairs repeating sequence model newly proposed leads to reasonable results for the UV, ORD, and CD spectral bandshapes.

The binding of dye molecules to some species of macro-biomolecules exhibits metachromasy, *i.e.*, appreciable change in the UV absorption spectra of the dye molecules. Such formation of molecular complexes often accompanies the extrinsically induced Cotton effect which usually appears in the corresponding UV absorption region of the dye. For instance, the interaction of nucleic acids with acridine dyes is the case for this phenomena. The spectral profiles for the UV, ORD, and CD bands of the DNA–dye and/or RNA–dye complexes remarkably change depending upon the several binding modes of the dyes to the polymers, which have specifically been discussed in terms of the phosphate/dye ($=P/D$) ratio in the literature. It is a hard task to analyze these profiles in detail, since there is a difficulty in properly assuming the definite models of conformation for such complicated molecular complexes. Nevertheless, there have been published several investigations on the bandshapes of biopolymer–dye complexes.[1-7]

In order to elucidate the spectral profiles, there have been mainly two models proposed; one is the outside-stacking model of dyes bound weakly to the phosphate groups corresponding to the case $P/D\approx 1$, and the other is the intercalation model in which monomeric dyes are strongly penetrated between the base-pairs corresponding to the case $P/D\gg 1$. In opposition to this, there is a finding that the latter model is good enough even for the low P/D ratio, for example $P/D=4$.[8] If we can clarify further detail of the bandshapes for these models in terms of Green's function method, some useful information which we might have discarded up to now will be expected to become available for the determination of unknown structures of biopolymer–dye complexes, including the mutual geometries among dyes and the binding sites of dyes. This paper is a mere trial but the first attempt to attain this aim. In our method, dye molecules play a roll as kinds of probes to see the structures of macromolecules in the bandshape analysis. In order to provide a theoretical foundation for analyzing these bandshapes of molecular complexes, we firstly need to prepare such a theoretical tool that is capable of being satisfactorily checked with a model polymer of known structure.

Recently, we have presented the linear response theory of the UV, ORD, and CD bandshapes for homopolymer systems[9-12] which has satisfactorily, to some extent, been applied to polyadenylic acid to which an X-ray analysis datum is available. By applying this theory to various models of the DNA–Acridine Orange (AO) complex, we compute the UV, ORD, and CD bandshapes in order for seeking possibilities of a further detailed analysis for such a complicated system.

Basic Formulas for Computing the UV, ORD, and CD Curves

The basic formulas necessary for the calculations of the UV, ORD, and CD bandshapes are collected below:

$$\boldsymbol{\alpha}_m^{\mathrm{M}}(\bar{\nu}) = \underset{(+)}{-}(hc)^{-1}\sum_{\lambda}\boldsymbol{\mu}_{0\lambda}^{(m)}\boldsymbol{\mu}_{\lambda 0}^{(m)}[(\bar{\nu}-\bar{\nu}_{\lambda 0}^{(m)}+i\eta_{\lambda}^{(m)})^{-1} - (\bar{\nu}+\bar{\nu}_{\lambda 0}^{(m)}-i\eta_{\lambda}^{(m)})^{-1}], \quad (1)$$

$$\boldsymbol{\alpha}_{mn}^{\mathrm{P}}(\bar{\nu}) = \boldsymbol{\alpha}_m^{\mathrm{M}}(\bar{\nu})\delta_{mn} \underset{(+)}{-} \boldsymbol{\alpha}_m^{\mathrm{M}}(\nu)\cdot\mathbf{U}_{mn}\cdot\boldsymbol{\alpha}_n^{\mathrm{M}}(\nu) + \sum_{l}^{\mathrm{N}}\boldsymbol{\alpha}_m^{\mathrm{M}}(\bar{\nu})\cdot\mathbf{U}_{ml}\cdot\boldsymbol{\alpha}_l^{\mathrm{M}}(\bar{\nu})\cdot\mathbf{U}_{ln}\cdot\boldsymbol{\alpha}_n^{\mathrm{M}}(\bar{\nu}) \underset{(+)}{-} \cdots, \quad (2)$$

$$\mathbf{U}_{mn} = \mathbf{1}_{mn}/r_{mn}^3 - 3\mathbf{r}_{mn}\mathbf{r}_{mn}/r_{mn}^5, \quad (3)$$

$$\mathbf{r}_{mn} = \mathbf{r}_n - \mathbf{r}_m = x_{mn}\mathbf{i} + y_{mn}\mathbf{j} + z_{mn}\mathbf{k}, \quad (4)$$

$$\beta(\bar{\nu}) = (1/12)\sum_{m}^{\mathrm{N}}\sum_{n}^{\mathrm{N}}\mathbf{r}_{mn}\cdot(\boldsymbol{\alpha}_{mn}^{\mathrm{P}}(\bar{\nu}):\boldsymbol{\varepsilon}), \quad (5)$$

$$\varepsilon_{xyz} = -\varepsilon_{xzy} = \varepsilon_{zxy} = -\varepsilon_{zyx} = \varepsilon_{yzx} = -\varepsilon_{yxz} = 1, \quad (6)$$

$$\varepsilon(\nu) = \underset{(-)}{+}(8\pi^2 N_{\mathrm{A}}/2302.6)\bar{\nu}[N^{-1}\sum_{m}^{\mathrm{N}}\sum_{n}^{\mathrm{N}}(1/3)\mathrm{Tr}\,\boldsymbol{\alpha}_{mn}^{\mathrm{P}}(\bar{\nu}), \quad (l\ \mathrm{mol}^{-1}\ \mathrm{cm}^{-1}), \quad (7)$$

$$[\Phi(\nu)] = \underset{(-)}{+}288\pi^2 N_{\mathrm{A}}\bar{\nu}^2[N^{-1}\mathrm{Re}\,\beta(\bar{\nu})], \quad (\mathrm{deg\ cm^2/dmol^{-1}}), \quad (8)$$

$$[\Theta(\nu)] = \underset{(-)}{+}288\pi^2 N_{\mathrm{A}}\bar{\nu}^2[N^{-1}\mathrm{Im}\,\beta(\bar{\nu})], \quad (\mathrm{deg\ cm^2/dmol^{-1}}). \quad (9)$$

The notations and units used above are just the same as those of our previous paper.[12] $\boldsymbol{\mu}_{0\lambda}^{(m)}\boldsymbol{\mu}_{\lambda 0}^{(m)}$ is a dyadic product of the transition moment between the λth excited state and the ground state of the mth monomer. To avoid confusion in the formulations which have appeared in the literature on this subject, it seems well to comment upon the sign convention. Depending upon the definition for the monomer polarizability tensor α_m^{M}, that is, either the minus or the plus signs before Eq. 1, the upper or the lower (parenthesized) signs in Eqs. 2, 7, 8, and 9 appear respectively. Although we have chosen the plus sign before Eq. 1 in our previous papers, the

minus sign in Eq. 1 is rather recommended because it is the customarily used definition. Another reason is that if we choose the minus sign in Eq. 1 the plus and the minus signs appear alternately in the expansion formula (Eq. 2) derived perturbatively from the classical electromagnetic theory,[13,14] Note that in the literature we sometimes find the opposite sign convention for $\mathbf{U}_{mn}$[15] which leads to Eq. 2 with all the plus signs even by using the conventional definition (minus) for Eq. 1.

Let us consider a biopolymer–dye complex in which the dyes are regularly arrayed and bound to the biopolymer one way or another. It is now assumed that experimentally and/or theoretically we will be able to know the monomer polarizability tensor $\boldsymbol{\alpha}^{\mathrm{p}}_{mn}(\bar{\nu})$ for the mth constituent dye chromophore bound to the biopolymer. Then, we can derive the matrix element of the polarizability tensor $\boldsymbol{\alpha}^{\mathrm{p}}_{mn}(\bar{\nu})$ for the biopolymer–dye complex, by using hypothetically a Dyson-type equation (Eq. 2). In Eq. 2, the interactions among the dyes and the macromolecular skeleton are neglected for simplicity. Actually, this means that the macromolecule–dye complex could be approximated as a polymer (N-mer) of aggregated dyes, in so far as we are concerned with the specific wavelength region of our interest.

From Eq. 2, we can calculate the UV absorbance $\varepsilon(\bar{\nu})$ and the optical rotatory parameter $\beta(\bar{\nu})$.[14] Different from our previous paper,[12] let us relate $\beta(\bar{\nu})$ of Eq. 5 with the familiar scalar triple product $\mathbf{r}_{mn}\cdot\boldsymbol{\mu}^{(m)}_{0\lambda}\times\boldsymbol{\mu}^{(n)}_{\lambda'0}$:

$$\begin{aligned}\beta(\bar{\nu}) &= (1/12)\sum_m^N\sum_n^N\sum_k(\mathbf{r}_{mn})_k\sum_t\sum_j\alpha^{\mathrm{P}ij}(\bar{\nu})\varepsilon_{jik}\\ &= -(1/12)\sum_m^N\sum_n^N\sum_i\sum_{j\neq k}(\mathbf{r}_{mn})_k(\alpha^{\mathrm{P}ij}_{mn}(\bar{\nu})-\alpha^{\mathrm{P}ji}_{mn}(\bar{\nu}))_k\\ &= -(1/12)\sum_m^N\sum_n^N[x_{mn}\vdots y_{mn}\vdots z_{mn}]\begin{bmatrix}\alpha^{\mathrm{P}yz}_{mn}(\bar{\nu})-\alpha^{\mathrm{P}zy}_{mn}(\bar{\nu})\\ \cdots\cdots\cdots\cdots\\ \alpha^{\mathrm{P}xz}_{mn}(\bar{\nu})-\alpha^{\mathrm{P}zx}_{mn}(\bar{\nu})\\ \cdots\cdots\cdots\cdots\\ \alpha^{\mathrm{P}xy}_{mn}(\bar{\nu})-\alpha^{\mathrm{P}yx}_{mn}(\bar{\nu})\end{bmatrix},\end{aligned}\tag{10}$$

where the symbol $(\ )_k$ denotes the kth component of the vector and $i,j,k=x,y,z$. Equation 10 is a working formula for the evaluation of $\beta(\bar{\nu})$, with simultaneous use of Eq. 2.

On the other hand, if we formally assume the polymer polarizability tensor as

$$\begin{aligned}\alpha^{\mathrm{P}}_{mn}(\bar{\nu}) = &-\underset{(+)}{(hc)^{-1}}\sum_\lambda\boldsymbol{\mu}^{\mathrm{P}(m)}_{0\lambda}\times\boldsymbol{\mu}^{\mathrm{P}(n)}_{\lambda 0}[(\bar{\nu}-\bar{\nu}^{\mathrm{P}}_{\lambda 0}+i\eta^{\mathrm{P}}_\lambda)^{-1}\\ &-(\bar{\nu}+\bar{\nu}^{\mathrm{P}}_{\lambda 0}-i\eta^{\mathrm{P}}_\lambda)^{-1}],\end{aligned}\tag{11}$$

Eq. 10 leads to the familiar formula for describing optical rotation:

$$\begin{aligned}\beta(\bar{\nu}) = &-\underset{(+)}{(-12hc)^{-1}}\sum_m^N\sum_n^N\sum_\lambda\mathbf{r}_{mn}\cdot\boldsymbol{\mu}^{\mathrm{P}(m)}_{0\lambda}\times\boldsymbol{\mu}^{\mathrm{P}(n)}_{\lambda 0}[(\bar{\nu}-\bar{\nu}^{\mathrm{P}}_{\lambda 0}+i\eta^{\mathrm{P}}_\lambda)]^{-1}\\ &-(\bar{\nu}+\bar{\nu}^{\mathrm{P}}_{\lambda 0}-i\eta^{\mathrm{P}}_\lambda)^{-1}],\end{aligned}\tag{12}$$

which indicates the conformationally induced exciton-type optical rotation. However, Eq. 12 contains unknown quantities relating to the polymer and can not be practically used for the evaluation of $\beta(\bar{\nu})$. Instead, going back to Eq. 5, we can derive the following equation to a first order approximation with respect to $\mathbf{U}_{mn}$ in Eq. 2:

$$\begin{aligned}\beta(\bar{\nu}) &= (1/12)\sum_m^N\sum_n^N\mathbf{r}_{mn}\cdot[\boldsymbol{\alpha}^{\mathrm{M}}_m(\bar{\nu}):\boldsymbol{\varepsilon}-\underset{(+)}{(\boldsymbol{\alpha}^{\mathrm{M}}_m(\bar{\nu})\cdot\mathbf{U}_{mn}\cdot\boldsymbol{\alpha}^{\mathrm{M}}_n(\bar{\nu}))}:\boldsymbol{\varepsilon}]\\ &= 0-\underset{(+)}{(12)^{-1}}\sum_m^N\sum_n^N\sum_k(\mathbf{r}_{mn})_k\sum_i\sum_j(\alpha^{\mathrm{M}}_m(\nu)\cdot\mathbf{U}_{mn}\cdot\alpha^{\mathrm{M}}_n(\nu))_{ij}\varepsilon_{jik}\\ &= -\underset{(+)}{(-12)^{-1}}(hc)^{-2}\sum_m^N\sum_n^N\sum_\lambda\sum_{\lambda'}(\boldsymbol{\mu}^{(m)}_{0\lambda}\cdot\mathbf{U}_{mn}\cdot\boldsymbol{\mu}^{(n)}_{\lambda' 0})\\ &\quad\times(\mathbf{r}_{mn}\cdot\boldsymbol{\mu}^{(m)}_{0\lambda}\times\boldsymbol{\mu}^{(n)}_{\lambda' 0})[(\bar{\nu}-\bar{\nu}^{(m)}_{\lambda 0}+i\eta^{(m)}_\lambda)^{-1}\\ &\quad-(\bar{\nu}+\bar{\nu}^{(m)}_{\lambda 0}-i\eta^{(m)}_\lambda)^{-1}][(\bar{\nu}-\bar{\nu}^{(n)}_{\lambda' 0}+i\eta^{(n)}_{\lambda'})^{-1}\\ &\quad-(\bar{\nu}+\bar{\nu}^{(n)}_{\lambda' 0}-i\eta^{(n)}_{\lambda'})^{-1}].\end{aligned}\tag{13}$$

Equation 13 does not contain any unknown polymer parameter and is found to be quite similar to the equations derived by Applequist[14] and Kirkwood *et al.*[16,17] Equations 12 and 13 are exactly the same formulas from a viewpoint of a first order approximation. However, we can preferentially make use of Eq. 13 when we wish to take higher order terms into account. For example, replacing $\mathbf{U}_{mn}$ in Eq. 13 with

$$\begin{aligned}\mathbf{U}_{mn} = \mathbf{U}_{mn} &+ \sum_t\mathbf{U}_{mt}\cdot\boldsymbol{\alpha}^{\mathrm{M}}_t\cdot\mathbf{U}_{tn}\\ &+ \sum_t\sum_s\mathbf{U}_{mt}\cdot\boldsymbol{\alpha}^{\mathrm{M}}_t\cdot\mathbf{U}_{ts}\cdot\boldsymbol{\alpha}^{\mathrm{M}}_s\cdot\mathbf{U}_{sn}+\cdots,\end{aligned}\tag{14}$$

we can to infinite order approximation describe $\beta(\bar{\nu})$ in terms of a sum of the product of the scalar triplet product $\mathbf{r}_{mn}\cdot\mu^{(m)}_{0\lambda}\times\mu^{(n)}_{\lambda' 0}$ and the intermonomer interaction $\boldsymbol{\mu}^{(m)}_{0\lambda}\cdot\mathbf{U}_{mn}\cdot\boldsymbol{\mu}^{(n)}_{\lambda' 0}$.

Infinite Orders Approximation for the Polymer Polarizability Tensor

In a previous calculation of the bandshapes of polyadenylic acid,[12] we took into account Eq. 2 up to the second order terms with respect to $\mathbf{U}_{mn}$. However, the expansion series of Eq. 2 very slowly converge in the case that chromophores have large transition moments, so that we must include higher order terms in Eq. 2 for the present calculation of the DNA–AO complex. It may rather be clever to choose the following computational scheme which involves the intermonomer interactions $\mathbf{U}_{mn}$ to infinite orders, since such a calculation in the expanded form of power series becomes time-consuming due to the increase in the number of overlappings of the *DO* loops in a computer program.

If we follow the upper sign convention in Eqs. 1, 2, 7, 8, and 9, Eq. 2 reduces to

$$\begin{aligned}\alpha^{\mathrm{P}} &= (1+\boldsymbol{\alpha}^{\mathrm{M}}\cdot\mathbf{U})^{-1}\boldsymbol{\alpha}^{\mathrm{M}}\\ &= \begin{bmatrix}\mathbf{1} & \boldsymbol{\alpha}^{\mathrm{M}}_1\cdot\mathbf{U}_{12}\cdots\boldsymbol{\alpha}^{\mathrm{M}}_1\cdot\mathbf{U}_{1N}\\ \boldsymbol{\alpha}^{\mathrm{M}}_2\cdot\mathbf{U}_{21} & \mathbf{1}\quad\cdots\boldsymbol{\alpha}^{\mathrm{M}}_2\cdot\mathbf{U}_{2N}\\ \cdots\cdots & \\ \boldsymbol{\alpha}^{\mathrm{M}}_N\cdot\mathbf{U}_{N1} & \boldsymbol{\alpha}^{\mathrm{M}}_N\cdot\mathbf{U}_{N2}\cdots\mathbf{1}\end{bmatrix}^{-1}\begin{bmatrix}\boldsymbol{\alpha}^{\mathrm{M}}_1 & \mathbf{0}\cdots\mathbf{0}\\ \mathbf{0} & \boldsymbol{\alpha}^{\mathrm{M}}_2\cdots\mathbf{0}\\ & \cdots\cdots\\ \mathbf{0} & \mathbf{0}\cdots\boldsymbol{\alpha}^{\mathrm{M}}_N\end{bmatrix},\end{aligned}\tag{15}$$

where

$$\mathbf{1}=\begin{bmatrix}1&0&0\\0&1&0\\0&0&1\end{bmatrix},\qquad\mathbf{0}=\begin{bmatrix}0&0&0\\0&0&0\\0&0&0\end{bmatrix}.\tag{16}$$

The tensor components of the 3×3 matrix for $\boldsymbol{\alpha}^{\mathrm{M}}_m(\bar{\nu})$ are given as

$$\alpha^{\mathrm{M}ij}_m(\bar{\nu}) = \mathrm{Re}\,\alpha^{\mathrm{M}ij}_m(\bar{\nu}) + i\mathrm{Im}\,\alpha^{\mathrm{M}ij}_m(\bar{\nu}),\quad(i,j=x,y,z),\tag{17}$$

and we finally obtain

$$\mathrm{Re}\,\alpha_m^{Mij}(\bar{\nu}) = -\sum_{\lambda}(hc)^{-1}[\mu_{0\lambda}^{(m)}]_i[\mu_{\lambda 0}^{(m)}]_j\{(\bar{\nu}-\bar{\nu}_{\cdot 0}^{(m)})[(\bar{\nu}-\bar{\nu}_{\lambda 0}^{(m)})^2 + \eta_\lambda^{(m)2}]^{-1} - (\bar{\nu}+\bar{\nu}_{\lambda 0}^{(m)})[(\bar{\nu}+\bar{\nu}_{\lambda 0}^{(m)})^2+\eta_\lambda^{(m)2}]^{-1}\}, \quad (18)$$

$$\mathrm{Im}\,\alpha_m^{Mij}(\nu) = +\sum_{\lambda}(hc)^{-1}[\mu_{0\lambda}^{(m)}]_i[\mu_{\lambda 0}^{(m)}]_j\{\eta_\lambda[(\bar{\nu}-\bar{\nu}_{\lambda 0}^{(m)})^2 + \eta_\lambda^{(m)2}]^{-1} + \eta_\lambda[(\bar{\nu}+\bar{\nu}_{\lambda 0}^{(m)})^2+\eta_\lambda^{(m)2}]^{-1}\}. \quad (19)$$

Being utilized the subroutine to compute the inverse of the $3N\times 3N$ complex matrix, the matrix elements $\alpha_{mn}^{p}(\bar{\nu})$ can easily be obtained, and then the three bandshape functions for the molar absorptivity (Eq. 7), molar rotation (Eq. 8), and molar ellipticity (Eq. 9) are computed by making use of Eqs. 10 and 15.

Specification of Models and Computational Procedures

As shown in Fig. 1, we assume such a regular model that the dyes are helically aggregated on the sites of the polymer skeleton. Here, the Cartesian coordinate is taken along the radial (r), tangential (t), and vertical (z) directions of the first dye monomer site considered. By doing so, we can relate the non-interacting monomer polarizability tensor of the mth site, $\boldsymbol{\alpha}_m^{M}(\bar{\nu})$, with that of the first site, $\boldsymbol{\alpha}_1^{M}(\bar{\nu})$:

$$\boldsymbol{\alpha}_m^{M}(\bar{\nu}) = \mathbf{R}[+(m-1)\phi]\cdot\boldsymbol{\alpha}_1^{M}(\bar{\nu})\cdot\mathbf{R}[-(m-1)\phi] = \mathbf{R}_z[-(m-1)\phi]\cdot\boldsymbol{\alpha}_1^{M}(\bar{\nu})\cdot\mathbf{R}_z[+(m-1)\phi], \quad (20)$$

where

$$\mathbf{R}(\phi) = \mathbf{R}_z(-\phi) = \begin{pmatrix} \cos\phi & -\sin\phi & 0 \\ \sin\phi & \cos\phi & 0 \\ 0 & 0 & 1 \end{pmatrix}. \quad (21)$$

For instance, if we put the first dye on the r',t'-plane determined by the parameters of angles such as $\theta°$, $tilt°$, and $twist°$ as depicted in Fig. 1, the components of the transition moment $\mu_{0\lambda}^{(1)}$ in the Cartesian coordinate are given by

$$\begin{bmatrix}[\mu_{0\lambda}^{(1)}]_r \\ [\mu_{0\lambda}^{(1)}]_t \\ [\mu_{0\lambda}^{(1)}]_z\end{bmatrix} = \mathbf{R}_t(+|twist|)\cdot\mathbf{R}_{r'}(-|titl|)\begin{bmatrix}[\mu_{0\lambda}^{(1)}]_{r'} \\ [\mu_{0\lambda}^{(1)}]_{t'} \\ [\mu_{0\lambda}^{(1)}]_{z'}\end{bmatrix} = \begin{bmatrix}\cos(+|twist|) & 0 & -\sin(+|twist|) \\ 0 & 1 & 0 \\ \sin(+|twist|) & 0 & \cos(+|twist|)\end{bmatrix} \times \begin{bmatrix}1 & 0 & 0 \\ 0 & \cos(-|tilt|) & \sin(-|tilt|) \\ 0 & -\sin(-|tilt|) & \cos(-|tilt|)\end{bmatrix}\begin{bmatrix}[\mu_{0\lambda}^{(1)}]_{r'} \\ [\mu_{0\lambda}^{(1)}]_{t'} \\ [\mu_{0\lambda}^{(1)}]_{z'}\end{bmatrix}. \quad (22)$$

By defining the plus sign of the angles counter-clockwise, we can write more generally

$$\begin{bmatrix}[\mu_{0\lambda}^{(1)}]_r \\ [\mu_{0\lambda}^{(1)}]_t \\ [\mu_{0\lambda}^{(1)}]_z\end{bmatrix} = \mathbf{R}_t[-|twist|\cdot\mathrm{sgn}(twist)]\cdot \mathbf{R}_{r'}[-|tilt|\cdot\mathrm{sgn}(tilt)]\begin{bmatrix}[\mu_{0\lambda}^{(1)}]_{r'} \\ [\mu_{0\lambda}^{(1)}]_{t'} \\ [\mu_{0\lambda}^{(1)}]_{z'}\end{bmatrix}. \quad (23)$$

Thus, we can compute the bandshapes by making use of Eqs. 7, 8, and 9 for either the outside-stacking or the intercalation model by changing the parameters (a, ϕ, $pitch$, θ, $tilt$, $twist$) as illustrated in Fig. 1.

With the scope of outside-binding models, we newly propose a dimerpairs repeating sequence model illustrated in Fig. 2. Looking at this model, every dye is

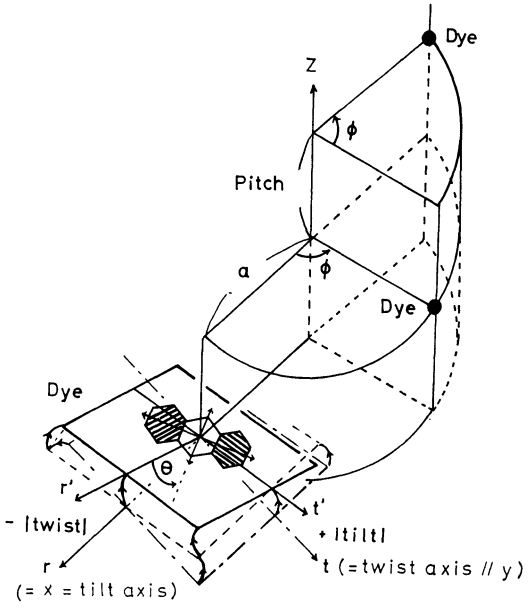

Fig. 1. A model of the Acridine Orange polymer helically stacked on the one-strand of DNA–AO complex and its geometrical parameters.

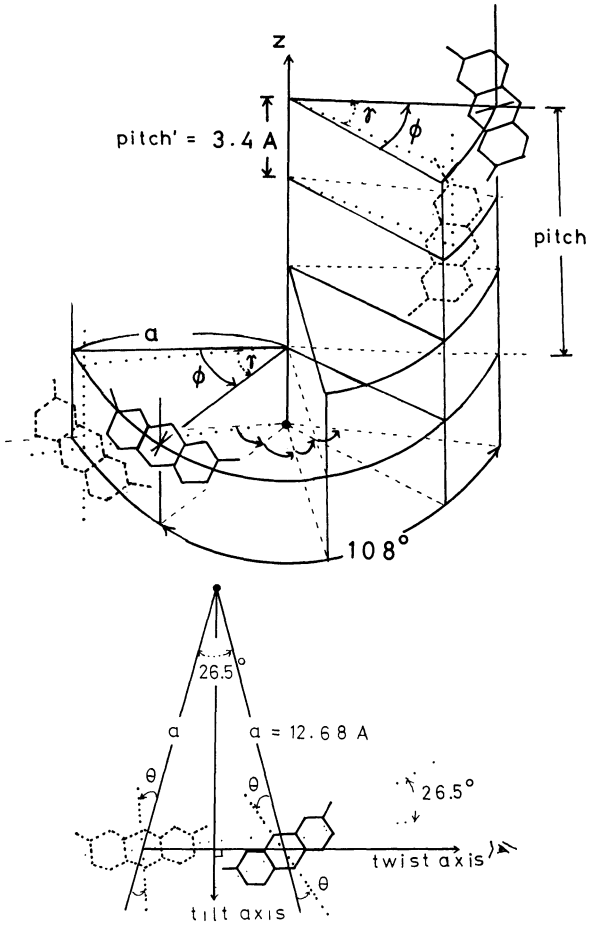

Fig. 2. A dimer-pairs repeating sequence model $[(\mathrm{dye})_2]_N$ for DNA–AO complex and its geometrical parameters.

found to be arrayed on the site of the same strand. However, if we change our views just for the computational convenience, we can readily regard this single-stranded polymer of the dyes as the double-stranded one, *i.e.*, one strand consisting of the dyes shown with the dotted line and another strand building from the dyes drawn with the solid line. This may be the special case of the double-stranded model shown in Fig. 1 of our previous paper.[12] In Table 1, the double-stranded DNA–AO polymer model presented by Tinoco *et al.*[1] is described by the parameters assigned in Fig. 2. Corresponding to Eq. 20 which defines the polarizability tensor of the mth monomer, the polarizability tensor of the m'th monomer can be obtained by a simple rotation from the position m, being assumed the geometry of the double-stranded DNA–AO complex, so as to satisfy

$$\boldsymbol{\alpha}^{M}_{m'}(\bar{\nu}) = \mathbf{R}(\gamma)\cdot\boldsymbol{\alpha}^{M}_{m}(\bar{\nu})\cdot\mathbf{R}(-\gamma), \quad (m' = \text{opposite site of } m), \tag{24}$$

and the position vectors are given by

$$\mathbf{r}_m = a\cos(m\phi)\hat{\mathbf{i}} + a\sin(m\phi)\hat{\mathbf{j}} + n\,\text{pitch}\,\hat{\mathbf{k}}, \tag{25}$$

$$\mathbf{r}_{m'} = a\cos(m\phi+\gamma)\hat{\mathbf{i}} + a\sin(m\phi+\gamma)\hat{\mathbf{j}} + (n\,\text{pitch}+\text{pitch}')\hat{\mathbf{k}}. \tag{26}$$

Results and Discussion

The spectroscopic parameters of the monomer dye, Acridine Orange, necessary for the calculations of the UV, ORD, and CD bandshapes of the polymer complex are experimentally determined as given in Table 1. In Table 2 are listed the various models assumed for the DNA–AO complex and the parameters describing the corresponding models. The results of model calculations are given through Fig. 3 to Fig. 10. In what follows, we are concerned specifically with the visible region of the whole bandshapes obtained. Tentatively, we assume that the dyes helically aggregate as if they were tilted and twisted in their molecular planes (see Fig. 1), with the parameters which are quite similar to the base parameters of the B-DNA geometry; *i.e.* *tilt*=2.1°, *twist*=−4.9°, *a* (variable in Å). Incidentally, the model presented by Tinoco *et al.*[1] corresponds to *tilt*=0.0°, *twist*=0.0°, *a*=12.68 Å. The assumption above implies that the molecular planes of the bound dyes are almost vertical to the helical axis of DNA, and in fact this nearly vertical orientation has experimentally been suggested.[19] It was shown in the study of polyadenylic acid[12] that the tilt and twist of the chromophores in the polymer system give rise to a large effect in the spectral bandshapes. We do not enter into the effect of tilting and twisting of the dyes beyond that, since there are some other unknown factors with regard to the parameters describing the DNA–AO complex.

Table 1. Spectroscopic parameters for the Acridine Orange monomer taken from the experimental data[a]

Energy $\frac{hc\bar{\nu}^{(m)}_{\lambda 0}}{\text{eV}}$	Oscillator strength $f_{\lambda 0}$	Damping factor[b] $\frac{\eta_\lambda}{\text{eV}}$	Polarization direction of transition moment
2.504	0.570	0.09540	long-axis
3.806	0.420	0.15475	long-axis
4.166	0.920	0.16297	long-axis
4.563	0.676	0.23062	short-axis

a) From Ref. 20. b) Estimated from Eq. 27 of Ref. 12.

Table 2. Various models for the DNA–AO complex and figure index

Fig. No.	Models	a Å	*tilt* degree	*twist* degree	ϕ degree	*pitch* Å	*pitch'* Å	γ degree	θ degree
3	Single-stranded intercalation[a] 5-mer	4.00	2.1	−4.9	72	6.80			36 40 45
4	Single-stranded outside-stacking *N*-mer (*N*=2, 3, 5, 11)	12.68	2.1	−4.9	36	3.40			52
5	5-mer	12.68 13.50 14.50	2.1	−4.9	36	3.40			90
6	Dimer	12.68	2.1	−4.9	36	3.40			40, 50, 60, 90
7	5-mer	12.68	2.1	−4.9	36	3.40			0, 35, 50, 55, 90
8	5-mer	12.68	2.1	−4.9	36	3.40			49, 50, 51, 52, 53, 54, 55
9	Double-stranded outside-stacking[b] 5-mer	12.68	0.0	0.0	36	3.40	2.72	−117.6	90
10	Outside-stacking *N*-dimer-pairs repeating sequence[c]								
	$(\text{Dye})_2$	12.68	2.1	−4.9	108	10.20	−3.40	−26.5[d]	55, 60
	$[(\text{Dye})_2]$	12.68	2.1	−4.9	108	10.20	−3.40	−26.5[d]	45, 55, 60

a) From Ref. 6. b) From Ref. 1. c) This model may be regarded as a single-stranded polymer of dyes rather than the double-stranded one. d) From the outside-stacking model proposed by Obendorf *et al.* (*a*=6 Å, ϕ=26.5°, *pitch*=4 Å).[21]

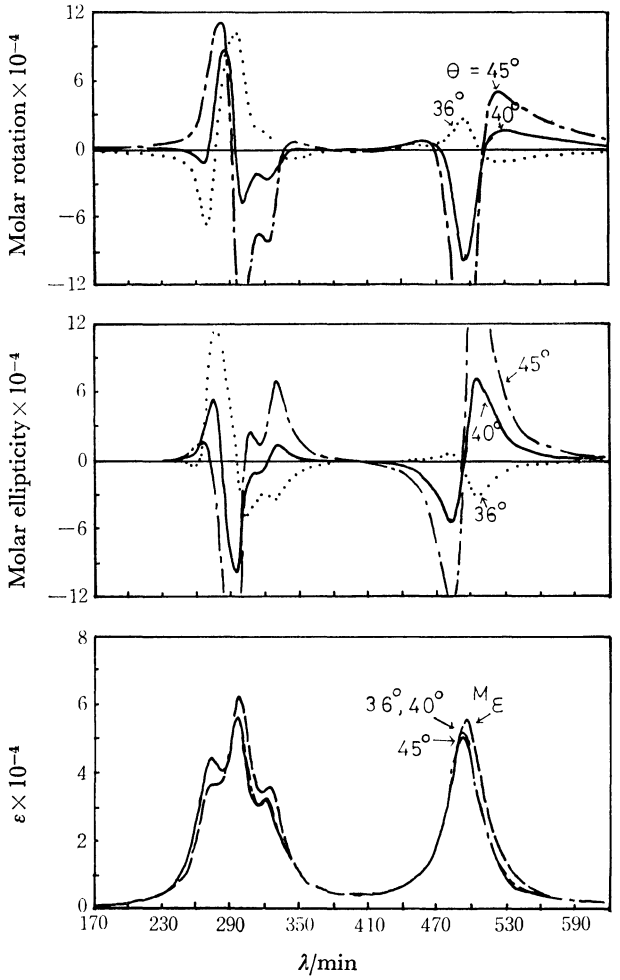

Fig. 3. The ORD (top), CD (middle), and UV (bottom) bandshapes for the intercalation model (see Table 2). $^{M}\varepsilon$ in the bottom shows the UV absorption spectrum of the AO monomer through Fig. 3 to Fig. 10.

Intercalation Model. Let us assume a simple model that the dyes are penetrated between every two base-pairs and constitute the single-stranded pentamer (5-mer) of the dyes as given in Table 2. This corresponds to the intercalation model for $P/D=4$—5. The spectral profiles computed with this model are shown in Fig. 3. In the visible region of the ORD and CD curves computed for the $\theta=40°$ model (see Fig. 1), we obtain the bandshapes having reasonable peaks and troughs in their spectral intensities in comparison with the curves of $P/D=5$ observed by Yamaoka and Resnik.[18] The first (longest wavelength) UV band computed shows only a minor blue shift and a slight decrease of intensity, even if whatever values are given for θ. Since the chain-length effect in the bandshapes is small even if we take N to be larger than 5 for the outside-stacking model (see below), qualitative feature to be obtained for the $N>5$ cases of the intercalation model might not be much different from Fig. 3. In short, in so far as the ORD and CD curves for low P/D ratios are concerned, the adequacy of this model is numerically proved. It seems that the feature of the first UV band observed for $P/D=5$ can qualitatively be reproduced for the specific θ-value ($\theta=40°$), though there still remains dissatisfaction about the intensity of the first UV band.

*Outside-stacking Models. Chain-length (*N*) Effect and Radius (*a*)-Dependence of the ORD, CD, and UV Bandshapes*: In Fig. 4, we investigated the chain-length effect of the bandshapes for the parameter $N=2$, 3, 5, 11 in the single-stranded models, fixing $\theta=52°$, which reproduces appropriately the ORD and CD curves. We found a tendency such that the computed curves for the $N=8$—11 models converge to certain shapes (approximately to that of the $N=5$ model). Therefore, for saving computational time, we carried out the model calculations of the DNA–AO complex only with the $N=2$ and $N=5$ species.

With a fixed θ-value $\theta=90°$, the dependence of the bandshapes for the single-stranded models upon the value of the radius, $a=12.68$, 13.5, and 14.5 Å, was examined as shown in Fig. 5. When we fix the parameters except the position of the binding site ($\vec{a}$), and make the value of $|\vec{a}|$ larger by degrees, the intermonomer interaction $\mathbf{U}_{mn}$ between the dyes becomes small, so that the ORD and CD curves decrease their

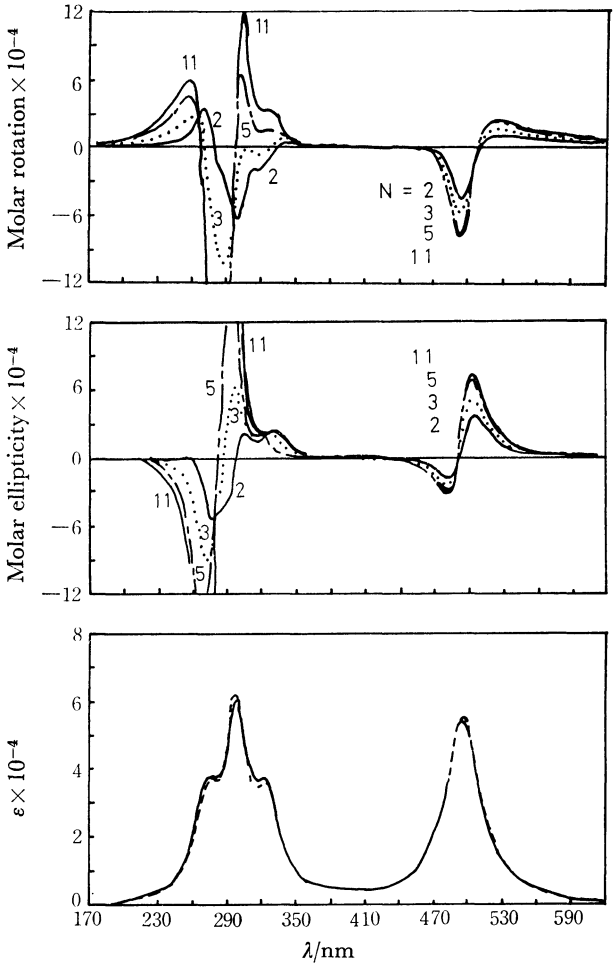

Fig. 4. The chain-length dependence ($N=2$, 3, 5, 11) of the ORD (top), CD (middle), and UV (bottom) bandshapes of the single-stranded outside-stacking N-mer model (see Table 2).

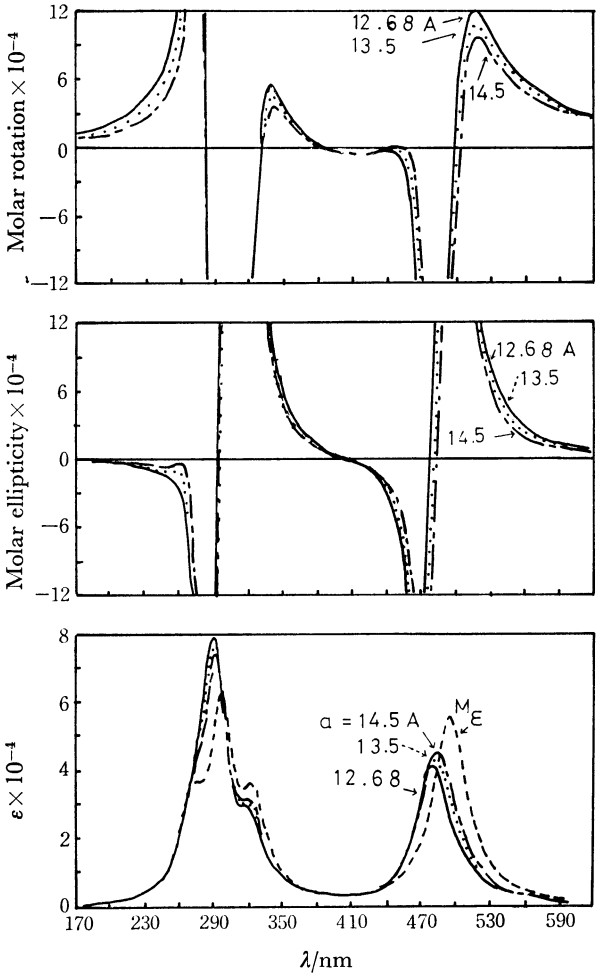

Fig. 5. Dependence of the ORD (top), CD (middle), and UV (bottom) bandshapes of the single-stranded outside-stacking 5-mer model (see Table 2) on the radius (a) of the helix.

intensities with the increase of $|\vec{a}|$ while the first UV band hardly change its peak and intensity. It is thus difficult to consider the possibility that the dyes will bind to the sites inside beyong the limit of 12.68 Å. For instance, in the stacking model presented by Obendorf *et al.*,[21] the binding site was set to be $|\vec{a}|=$ 6 Å and other parameters adopted were quite similar to our values. From Fig. 5, it is predicted that their model is indisputably denied.

Single-Stranded Dimer Model: From comparison of Figs. 4, 6, 7, and 8 it can be concluded that the qualitative feature of the UV, ORD, and CD bandshapes computed for the dimer does not very much change even for the $N>3$ polymers. In other words, the qualitative feature of these bandshapes in the visible region is mainly determined by the nearest neighbor interactions of the dyes with the intermonomer distance nearly equal to 3.4 Å. This suggestion also coincides with the experimental conclusion for the complexes of the low P/D ratios that the main binding species are dimeric molecules bound to the outside sites, while for those of $P/D\gg1$, it is usually accepted that the main binding species are monomeric. From our calculation, we have confidence in suggesting a model such that not the monomeric but the dimeric dyes are sparsely dispersed on the binding sites. If this assumption is correct, such a dimer model flexibly applies to the cases for $P/D\approx1$ as well as $P/D\gg1$. However, if this dimeric model is denied for $P/D\gg1$, we must consider that the optical activity may be induced not only by the local steric interaction between the monomeric dye and the base-pair (*i.e.*, conformationally induced optical activity), but also by the interaction between the dye and the sugar phosphate groups (*i.e.*, the intrinsic optical activity induced by the assymmetric environments). This monomeric binding is certainly the consensus ascertained experimentally for $P/D\gg1$. We do not carry out possible model calculations taking account of such effects, since there is no definite experimental datum in the shorter wavelength region available.

In Fig. 6, the model calculation for $\theta=90°$ gives the reasonable blue shift and intensity descent in the first UV band which are comparable to the bandshapes experimentally observed for $P/D=2$—5.[18] On the other hand, the calculation for $\theta=50°$ gives the reasonable ORD and CD curves for the corresponding experimental curves.[18] We could not find out a proper θ-value so as

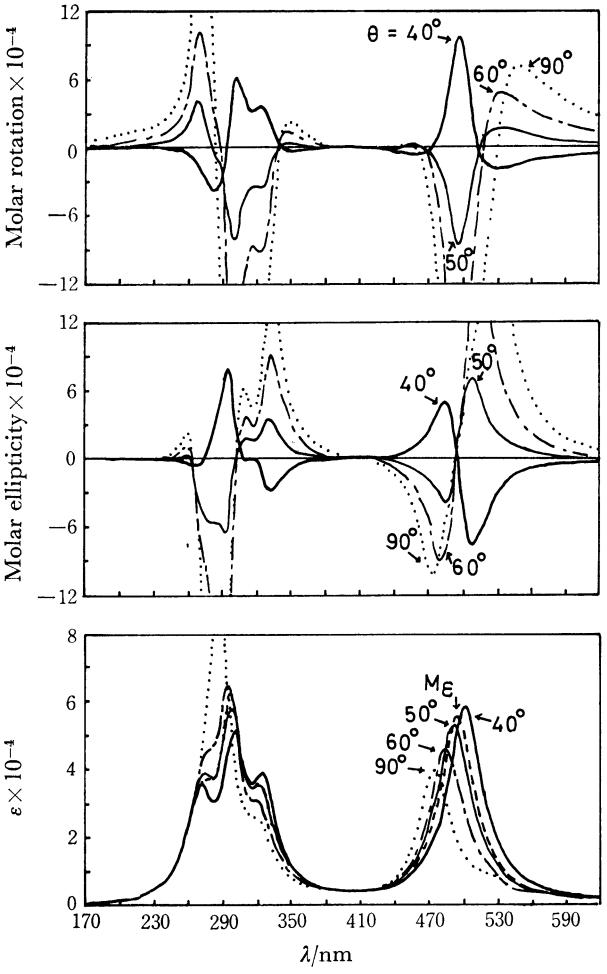

Fig. 6. The ORD (top), CD (middle), and UV (bottom) bandshapes for the outside-stacking dimer model (see Table 2).

to obtain the agreement of the computed UV, ORD, and CD bandshapes with experiments at the same time. It should be noticed that for $0°\leq\theta\leq40°$ the red shift and the intensity ascent are observed in the first UV band and that the reversed Cotton effect and the red shift in the ORD and CD bands come to be large. Such bandshapes computed happen to correspond to the experimental ones for $P/D\gg1$ and may be true if the species of the dimeric dyes are dispersedly bound to DNA. However, we must not forget that depending upon the experimental condition the reversed Cotton effect can be seen even for $P/D\approx1$.[6,22]

Single- and Double-Stranded 5-mer Models: As will be expected from the discussion of the chain-length effect, we obtain almost the same results in Fig. 7 as those in Fig. 6. The model calculation for $\theta=90°$ (the radial orientation of the long axis of the dye molecule) gives the reasonable blue shift and intensity descent which are comparable with the first UV band observed for the low P/D ratios, but the ORD and CD curves computed are too intense in comparison with the experimental ones. Our previous study[20] on the shift of the UV band suggested the radial orientation, but found that although the qualitative feature of the bandshapes is satisfied,[5] the ORD curves computed are extraordinarily strong in their intensites which may be brought about just due to the assumption of a smaller value of $|\vec{a}|=9.1$ Å compared with $|\vec{a}|=12.68$ Å, as is readily understood from the present results. On the other hand, the model calculation for $\theta=0°$ (tangential orientation of the long axis) gives a large red shift and a large reversed Cotton effect.

In Fig. 7, it should be noticed that the single-stranded models for $\theta=50°$—$55°$ give the ORD and CD curves comparable for the experimental ones of the low P/D ratios, while we have only the imperceptible UV intensity descent. When we compute the bandshapes in more detail, particularly for $\theta=49°$—$55°$ using the same model, we obtain the results as shown in Fig. 8. It is interesting to note that drastic changes of the ORD and CD curves occur for small changes in the vicinity of a specific value $\theta=55°$, and that the UV bandshape computed changes a little comparing with the experimental UV band.

By using the model presented by Tinoco *et al.*,[1] we computed the bandshapes for the single- and double-stranded DNA–AO complexes fixing $\theta=90°$, which are shown in Fig. 9. In this calculation, we used the spectral

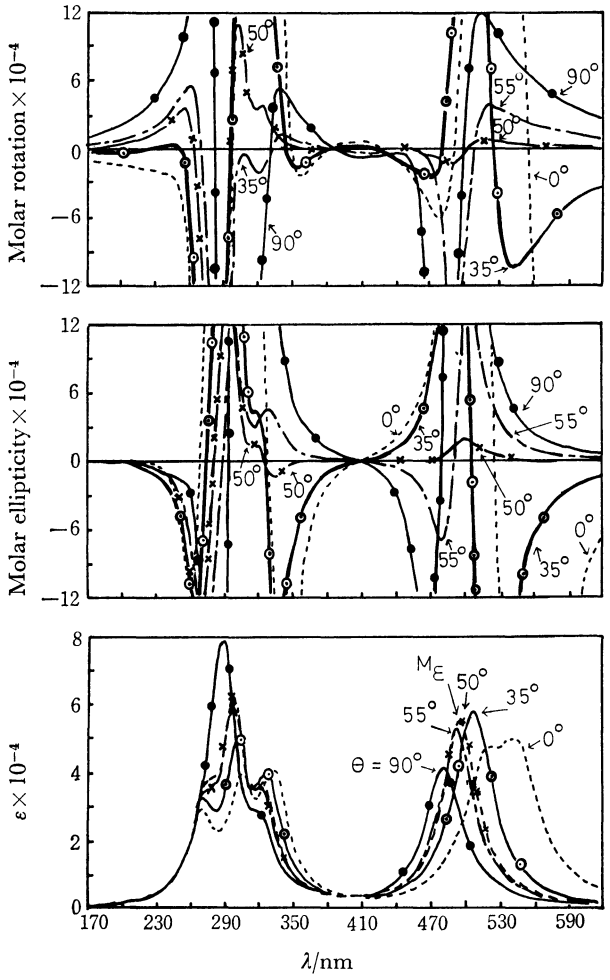

Fig. 7. Dependence of the ORD (top), CD (middle), and UV bottom) bandshapes for the outside-stacking 5-mer model (see Table 2) on the twisting angle (θ) of the short axis of the AO dye from the radial direction of the helix.

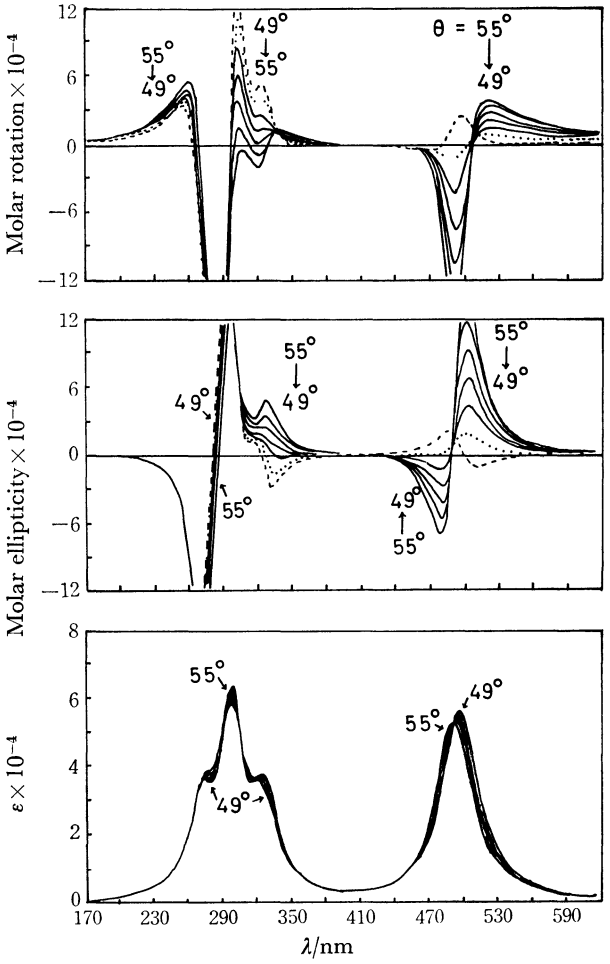

Fig. 8. The selected θ-dependence of the ORD (top), CD (middle), and UV (bottom) bandshapes for the single-stranded outside-stacking 5-mer model (see Table 2).

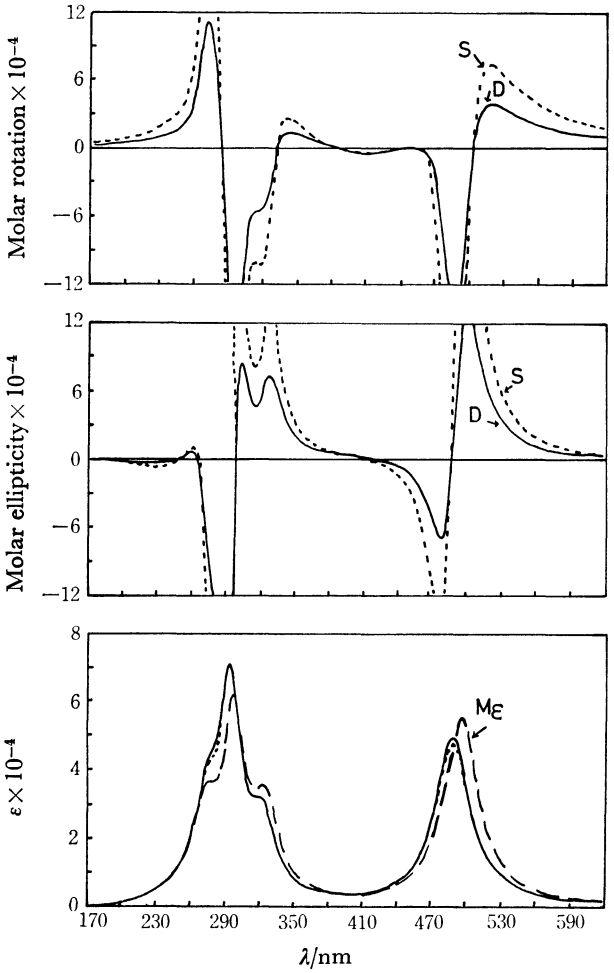

Fig. 9. The ORD (top), CD (middle), and UV (bottom) bandshapes for the single-stranded 5-mer model (see Table 2) similar to the Tinoco-Woody-Bradley model. The S and D denote the single- and double-strands, respectively.

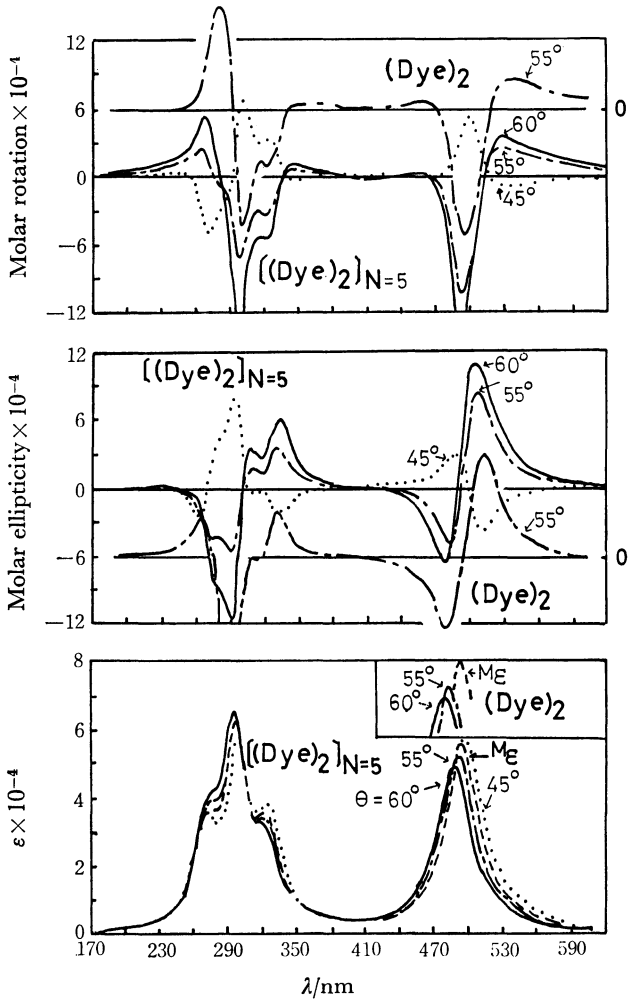

Fig. 10. The ORD (top), CD (middle), and UV (bottm) bandshapes for the one dimer-pair $(Dye)_2$ and/or the five dimer-pairs repeating sequence models $[(Dye)_2]_5$ (see Table 2).

parameters given in Table 1 and the screened potential $\mathbf{U}_{mn}^{\text{screen}}=(1/\varepsilon)\mathbf{U}_{mn}^{\text{bare}}$ with the dielectric constant $\varepsilon=2.0$, instead of the bare interaction $\mathbf{U}_{mn}=\mathbf{U}_{mn}^{\text{bare}}$. If we assume that the radial orientation ($\theta=90°$) of the dyes is experimentally correct, the discrepancy mentioned about Figs. 7 and 8 is found to be overcome in Fig. 9 by the inclusion of the dielectric screening effect and the dye-dye interaction between the double strands. However, ε is simply the parameter assumed tentatively and it may be difficult to choose the value which has a real physical meaning. We notice in Fig. 9 that the qualitative feature of the bandshapes for the single-stranded polymer is not definitely changed by allowing for the dye-dye interaction between the double strands. Concerning this model, there also remains dissatisfaction with regard to the fact that the extent of the blue shift and the intensity descent in the first UV band is small compared with the experimental bandshapes for the low P/D ratios.

Dimer-Pairs Repeating Sequence Model: For the dimer model mentioned in the previous paragraphs, we assume a rather different model as shown in Fig. 2 and in the bottom line of Table 2, which we call a dimer-pairs repeating sequence model. It is necessary to note that the model drawn in Fig. 2 is a kind of visualization of an external association model of dimer dyes, *i.e.*, the polymer of the dimer units which was used by Imae and Ikeda[6] for the calculations of CD curves. As shown in Fig. 10, the $(Dye)_2$- and $[(Dye)_2]_5$-models for $\theta=55°$ and 66° give the similar bandshapes, which are approximately comparable with the UV, ORD, and CD bandshapes observed for the low P/D ratios. For the models within the range $0°\leq\theta\leq45°$, the reversed Cotton effect can be seen in the visible region, and only small intensity increase and red shift in the first UV band are observed.

From the discussions mentioned above, it is found that the outside-stacked *one* dimer-pair model and/or the outside-stacked *five* dimer-pairs repeating sequence model is a good example to be able to well predict the experimental UV, ORD, and CD bandshapes for the low P/D ratios, as far as the models assumed in Table 2 are concerned. We obtain the reasonable bandshapes for the intercalation models of the low P/D ratio ($P/D=5$), but in the present paper we do not consider the possible intercalation models for $P/D\gg1$.

There still remain a lot of problems such as the correct assignment of the transition energies and the polarization directions of the transitions for the monomer dye, the introduction of the bandshape functions involving the vibrational levels, and the suitable determination of the damping factors ($=\Gamma/2$) of the monomer band governing the bandshapes of the polymer. The study on this line is now in progress.

References

1) I. Tinoco, Jr., R. W. Woody, and D. F. Bradley, *J. Chem. Phys.*, **38**, 1317 (1963).
2) D. F. Bradley, I. Tinoco, Jr., and R. W. Woody, *Biopolymers*, **1**, 239 (1963).
3) M. R. Philpott, *J. Chem. Phys.*, **53**, 968 (1970).
4) M. R. Philpott, *J. Chem. Phys.*, **54**, 4223 (1971).
5) Y. J. I'Haya, T. Nakamura, Y. Yagi, T. Sano, and H. Ito, *Int. J. Quantum Chem., Symp.*, **5**, 361 (1971).
6) I. Imae and S. Ikeda, *Polym. J.*, **8**, 531 (1976).
7) T. Imae and S. Ikeda, *Biopolymers*, **15**, 1655 (1976).
8) J. H. Perrin and P. A. Hart, *J. Pharm. Sci.*, **59**, 431 (1970) and references cited therein.
9) H. Ito, T. Eri, and Y. J. I'Haya, *Chem. Phys.*, **8**, 68 (1975), **10**, 497 (1975).
10) H. Ito, T. Eri, and Y. J. I'Haya, *Chem. Phys. Lett.*, **39**, 150 (1976), **45**, 610 (1977).
11) H. Ito and Y. J. I'Haya, 26th IUPAC Congress Abstracts (Tokyo, September 4—10, 1977) Sessions II and III, p. 594.
12) H. Ito, Y. J. I'Haya, and T. Eri, *Bull. Chem. Soc. Jpn.*, **51**, 1341 (1978).
13) C. J. Böttcher (1973), "Theory of Electric Polarizability," p. 208, Elsevier Scientific Publishing Company.
14) J. Applequist, *J. Chem. Phys.*, **58**, 4251 (1973).
15) A. R. Zib and W. Rhodes, *J. Chem. Phys.*, **57**, 5354 (1972).
16) J. G. Kirkwood, *J. Chem. Phys.*, **5**, 479 (1937).
17) W. W. Wood, W. Fickett, and J. G. Kirkwood, *J. Chem. Phys.*, **20**, 561 (1952).
18) K. Yamaoka and R. A. Resnik, *J. Phys. Chem.*, **70**, 4051 (1966).
19) S. F. Mason and A. J. McCaffery, *Nature*, **204**, 468 (1964).
20) H. Ito and Y. J. I'Haya, *Int. J. Quantum Chem.*, **2**, 5 (1968).
21) O. K. Obendorf, J. P. Glusker, P. R. Hansen, H. M. Berman, and H. L. Carrell, *Bioinorg. Chem.*, **6**, 29 (1976).
22) D. M. Neville, Jr., and D. F. Bradley, *Biochim. Biophys. Acta*, **50**, 397 (1961).